Journal of Power and Energy Engineering, 2025, 13(1), 18-31
https://www.scirp.org/journal/jpee
ISSN Online: 2327-5901
ISSN Print: 2327-588X

Output Voltage Stabilization of Non-Ideal DC-DC Zeta Converter with Output Voltage Error Elimination via Hybrid Control

Hafez Sarkawi[1], Noridah Mohd Ridzuan[2], Muhammad Idzdihar Idris[1], Mohd Syafiq Mispan[1]

[1]Fakulti Teknologi dan Kejuruteraan Elektronik dan Komputer, Universiti Teknikal Malaysia Melaka, Melaka, Malaysia
[2]Proton Advanced Automotive Technology Institute, Melaka, Malaysia
Email: hafez@utem.edu.my

How to cite this paper: Sarkawi, H., Ridzuan, N.M., Idris, M.I. and Mispan, M.S. (2025) Output Voltage Stabilization of Non-Ideal DC-DC Zeta Converter with Output Voltage Error Elimination via Hybrid Control. *Journal of Power and Energy Engineering*, **13**, 18-31.
https://doi.org/10.4236/jpee.2025.131002

Received: December 12, 2024
Accepted: January 23, 2025
Published: January 26, 2025

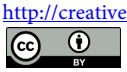

Abstract

In this paper, we proposed an output voltage stabilization of a DC-DC Zeta converter using hybrid control. We modeled the Zeta converter under continuous conduction mode operation. We derived a switching control law that brings the output voltage to the desired level. Due to infinite switching occurring at the desired level, we enhanced the switching control law by allowing a sizeable output voltage ripple. We derived mathematical models that allow one to choose the desired switching frequency. In practice, the existence of the non-ideal properties of the Zeta converter results in steady-state output voltage error. By analyzing the power loss in the zeta converter, we proposed an improved switching control law that eliminates the steady-state output voltage error. The effectiveness of the proposed method is illustrated with simulation results.

Keywords

Continuous Conduction Mode, DC-DC Zeta Converter, Hybrid Control, Output Voltage Error, Switching Control Law, Switching Frequency

1. Introduction

Energy harvesting systems have a power management system that includes a DC-DC converter. Because of the uncertain nature of the ambient energy, for example, low or high irradiance of the sun and fluctuation of the wind speed, the voltage generated by the energy harvester, which is connected to the input of the DC-DC converter, can possibly be higher or lower than the output voltage. For that reason, the fourth-order DC-DC converter is a good candidate for deployment since it

has step-up or step-down capability. There are a few topologies available, and the selection of a suitable topology is based on the intended application. With a smartphone battery charging application in mind where a solar panel gives the input, a suitable topology is the Zeta topology due to two reasons: 1) positive output voltage and low output voltage ripple, 2) natural DC input-to-output voltage isolation. The DC input in the zeta is disconnected/isolated from the output part in one of the two operation modes, precisely when the transistor is turned off. This isolation is beneficial, especially in uncertain solar energy sources, since it can reduce the effect of input voltage fluctuations.

There are several pulse width modulation (PWM)-based control techniques presented in the literature to control the DC-DC converter. The one most widely used is proportional integral (PI) control [1]-[5]. Although PI control produces fast output voltage regulation, it suffers from high control effort for the control duty-ratio [6] which can cause problems to the PWM circuitry. Another well-known controller is optimal control [6]-[11]. Conventional optimal linear quadratic regulator (LQR) control [6] [7] produces optimal compensation with minimal control effort. The downside, however, is that when the parameters have high uncertainty, the controller loses the capability to regulate the output. In [8]-[12], the authors consider the uncertainties in control design formulation and the controller can cope with large uncertainties at the expense of lower performance in nominal conditions. Other types of PWM-based controllers are sliding-mode [13]-[15], fuzzy [16] [17], adaptive [18] [19], and fuzzy-neural [20] [21], to name a few. The main disadvantage of the PWM-based controller is the high inrush current at the inductor during start-up due to the high switching frequency.

Hybrid control is a variable switching frequency type of controller. Hybrid control produces a low switching frequency at start-up; thus, the inrush current can be kept small. In [22]-[29], the authors used hybrid control to regulate the output voltage of buck [22], boost [23] [24] and buck-boost [25] converter by observing the relation between output voltage ripple and inductor current ripple. The fact that zeta topology has a very low output voltage ripple makes this method unsuitable. Control Lyapunov-based hybrid control is presented in [26]-[29]. Even though the output voltage is stabilized, the authors do not consider non-ideal conditions thus the output voltage error is not eliminated. In this paper, we propose hybrid control and consider non-ideal Zeta converter by including the transistor on resistance, equivalent series resistance for the two inductors, and forward voltage drop of the diode. By relating to the non-ideal condition and power loss, we introduced an improved hybrid control strategy that not only stabilized the Zeta converter, but also removed the steady-state output voltage error.

The remainder of the paper is organized as follows: In Section 2, we show the DC-DC Zeta converter modeling. In Section 3, we formulate a hybrid control strategy for the ideal and non-ideal Zeta converter. A design example and simulation results are given in Section 4. Lastly, in Section 5, we conclude our work.

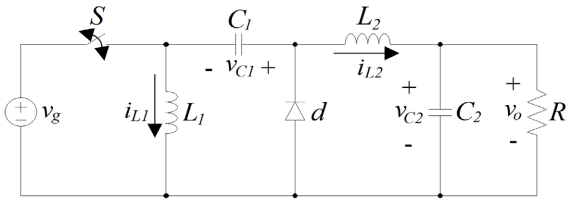

Figure 1. DC-DC Zeta converter circuit.

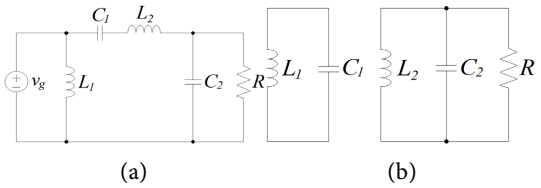

Figure 2. DC-DC Zeta converter equivalent circuit for (a) Mode 1, and (b) Mode 2.

2. DC-DC Zeta Converter CCM Model

Consider the DC-DC Zeta converter circuit shown in Figure 1. The circuit consists of two inductors L_1 and L_2, two capacitors C_1 and C_2, an ideal diode d and C_2, a DC voltage source v_g, a resistive load R, and an ideal switch S. Denote the currents of L_1 and L_2 as i_{L1} and i_{L2}, the voltages of C_1 and C_2 as v_{C1} and v_{C2}, respectively. Consider continuous conduction mode (CCM) operation of the converter. When the switch is closed (Mode 1), the converter is equivalent to the circuit shown in Figure 2(a), and when the switch is open (Mode 2), the converter is equivalent to the circuit shown in Figure 2(b). The state-space equation for the DC-DC Zeta converter is constructed using the state vector [29]

$$x = \begin{bmatrix} i_{L1} \\ i_{L2} \\ v_{C1} \\ v_{C2} \end{bmatrix},$$

and the input $u = v_g$:

$$\frac{\mathrm{d}x}{\mathrm{d}t} = A_k x + B_k u, \tag{1}$$

where $k = 1, 2$ represents the operation mode; $k = 1$ if the switch is closed (Mode 1) and $k = 2$ if the switch is open (Mode 2):

$$A_1 = \begin{bmatrix} 0 & 0 & 0 & 0 \\ 0 & 0 & \frac{1}{L_2} & -\frac{1}{L_2} \\ 0 & -\frac{1}{C_1} & 0 & 0 \\ 0 & \frac{1}{C_2} & 0 & -\frac{1}{RC_2} \end{bmatrix}, \quad B_1 = \begin{bmatrix} \frac{1}{L_1} \\ \frac{1}{L_2} \\ 0 \\ 0 \end{bmatrix}, \tag{2}$$

$$A_2 = \begin{bmatrix} 0 & 0 & -\frac{1}{L_1} & 0 \\ 0 & 0 & 0 & -\frac{1}{L_2} \\ \frac{1}{C_1} & 0 & 0 & 0 \\ 0 & \frac{1}{C_2} & 0 & -\frac{1}{RC_2} \end{bmatrix}, \quad B_2 = \begin{bmatrix} 0 \\ 0 \\ 0 \\ 0 \end{bmatrix}, \tag{3}$$

With the DC-DC Zeta converter model having been presented, the formulation of the switching control is addressed in the next section.

3. Hybrid Switching Control Formulation

The aim of the control is to design the switching law of S in such a way that the voltage of the load R becomes a prescribed value v_{ref}. For the DC-DC Zeta converter case, the steady-state operation point [29] is given by

$$x^* = \begin{bmatrix} i_{L1}^* \\ i_{L2}^* \\ v_{C1}^* \\ v_{C2}^* \end{bmatrix} = \begin{bmatrix} \frac{v_{ref}^2}{Rv_g} \\ \frac{v_{ref}}{R} \\ v_{ref} \\ v_{ref} \end{bmatrix}. \tag{4}$$

3.1. Ideal DC-DC Zeta Converter Control

Choose a control Lyapunov function (CLF) candidate

$$V(x) = (x - x^*)^{\mathrm{T}} P (x - x^*), \quad P = \mathrm{diag}\left\{\frac{L_1}{2}, \frac{L_2}{2}, \frac{C_1}{2}, \frac{C_2}{2}\right\}. \tag{5}$$

Let $\alpha_1(x)$ and $\alpha_2(x)$ be the derivative along the trajectory under Mode 1 and Mode 2, respectively. Then

$$\alpha_1(x) = -\frac{1}{R}\left(v_{C2}^* - v_{C2}\right)^2 + v_g\left(i_{L1} - i_{L1}^*\right) + v_g\left(i_{L2} - i_{L2}^*\right) - \frac{v_{ref}}{R}\left(v_{C1} - v_{C1}^*\right), \tag{6}$$

$$\alpha_2(x) = -\frac{1}{R}\left(v_{C2}^* - v_{C2}\right)^2 - \frac{v_{ref}}{v_g}\left(v_g\left(i_{L1} - i_{L1}^*\right) + v_g\left(i_{L2} - i_{L2}^*\right) - \frac{v_{ref}}{R}\left(v_{C1} - v_{C1}^*\right)\right). \tag{7}$$

Based on the CLF (5), we define the switching control law as follows:

Switching Control Law 1
When the current mode is Mode 1, if $\alpha_1(x) < 0$, then stay in Mode 1, otherwise change to Mode 2. When the current mode is Mode 2, if $\alpha_2(x) < 0$, then stay in Mode 2, otherwise change to Mode 1.

Direct implementation of *Switching Control Law* 1 however induces infinite

switching at the operating point which is impossible in practice. To overcome this problem, we propose an improved *Switching Control Law* 2 that makes the steady-state switching frequency finite.

Switching Control Law 2

When the current mode is Mode 1, if $\alpha_1(x) < \beta_1$, then stay in Mode 1, otherwise change to Mode 2.
When the current mode is Mode 2, if $\alpha_2(x) < \beta_2$, then stay in Mode 2, otherwise change to Mode 1.

With $\beta_1 > 0$ (under Mode 1) and $\beta_2 > 0$ (under Mode 2), the state-trajectory will move around the operating point where the states i_{L1}, i_{L2}, v_{C1}, and v_{C2}, are bounded by sizeable ripples. As a result, the switching is delayed, and since the switching time is inversely proportional to the switching frequency, the switching frequency is therefore reduced.

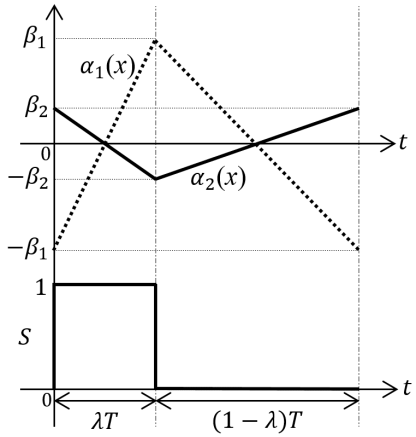

Figure 3. Approximate state-trajectory (top) and it's respected switching signal (bottom) at the steady-state.

Define $f = 1/T$ as the steady-state switching frequency and $\lambda = \dfrac{v_{ref}}{v_{ref} + v_g}$.

The derivative of $\alpha_1(x)$ and $\alpha_2(x)$ is given by

$$\dot{\alpha}_1(x) = \frac{2}{C_2 R^2}\left(v_{C2} - v_{C2}^*\right)^2 - \frac{2}{C_2 R}\left(v_{C2} - v_{C2}^*\right)\left(i_{L2} - i_{L2}^*\right) + \frac{i_{L2}^*}{C_1} i_{L2} + \frac{v_g}{L_2} v_{C1} - \frac{v_g}{L_2} v_{C2} + v_g^2\left(\frac{1}{L_1} + \frac{1}{L_2}\right),$$

$$\dot{\alpha}_2(x) = \frac{2}{C_2 R^2}\left(v_{C2} - v_{C2}^*\right)^2 - \frac{2}{C_2 R}\left(v_{C2} - v_{C2}^*\right)\left(i_{L2} - i_{L2}^*\right) + \frac{i_{L1}^*}{C_1} i_{L1} + \frac{v_{ref}}{L_1} v_{C1} + \frac{v_{ref}}{L_2} v_{C2}$$

Substituting $x = x^*$, then the gradient at the operating point is given by

$$\dot{\alpha}_1\left(x^*\right)=\frac{v_g^2}{L_1}+\frac{v_g^2}{L_2}+\frac{v_{ref}^2}{C_1R^2},$$

$$\dot{\alpha}_2\left(x^*\right)=\frac{v_{ref}^2}{v_g^2}\left(\frac{v_g^2}{L_1}+\frac{v_g^2}{L_2}+\frac{v_{ref}^2}{C_1R^2}\right).$$

Observing **Figure 3**, it is found that

$$\beta_1=\frac{\dot{\alpha}_1\left(x^*\right)\lambda}{2f}=\frac{v_{ref}\left(L_1L_2v_{ref}^2+C_1L_1R^2v_g^2+C_1L_2R^2v_g^2\right)}{2fC_1L_1L_2R^2\left(v_{ref}+v_g\right)}, \tag{8}$$

$$\beta_2=\frac{\dot{\alpha}_2\left(x^*\right)(1-\lambda)}{2f}=\frac{v_{ref}^2\left(L_1L_2v_{ref}^2+C_1L_1R^2v_g^2+C_1L_2R^2v_g^2\right)}{2fC_1L_1L_2R^2v_g\left(v_{ref}+v_g\right)}. \tag{9}$$

From (8) and (9) above, by defining the desired steady-state switching frequency f, *Switching Control Law* 2 will enforce the voltage regulation and makes the DC-DC Zeta converter operate at the prescribed switching frequency.

3.2. Non-Ideal DC-DC Zeta Converter Control

In practice, there exists an internal resistance or a voltage drop at the electronics components. Under this circumstance, the average input power P_{in} for the converter is given by $P_{\text{in}}=P_{\text{out}}+P_{\text{loss}}$, where P_{out} and P_{loss} is the output power, and the loss power, respectively. Since $P_{\text{out}}<P_{\text{in}}$, then

$$i_ov_o<i_{L1}^*v_g$$

$$\frac{v_o}{R}v_o<\frac{v_{ref}^2}{Rv_g}v_g$$

$$v_o<v_{ref}.$$

As shown above, the output voltage is less than the prescribed value. To compensate for the output voltage discrepancy, extra input power needs to be supplied. Consider the output voltage equal to the prescribed value. With the assumption of constant input current, the input voltage, therefore, needs to be increased, consequently the power loss is expressed by

$$\begin{aligned}P_{\text{loss}}&=P_{\text{in}}-P_{\text{out}}\\&=\frac{v_{ref}^2}{Rv_g}\left(v_g+\Delta v_g\right)-\frac{v_{ref}^2}{R}.\\&=\frac{\Delta v_g}{v_g}\frac{v_{ref}^2}{R}\end{aligned} \tag{10}$$

Dividing (8) and (9), the ratio of β_1 over β_2 is given by

$$\frac{\beta_1}{\beta_2}=\frac{v_g}{v_{ref}}. \tag{11}$$

For the Zeta topology, since the input voltage is only connected during Mode 1, the increase in the input voltage is therefore translated to the increment of β_1.

Let define

$$\frac{\beta_1'}{\beta_2} = \frac{v_g + \Delta v_g}{v_{ref}}. \tag{12}$$

Eliminating β_2 in (11) and (12), and solving for β_1' yield

$$\beta_1' = \beta_1 \left(1 + \frac{\Delta v_g}{v_g}\right).$$

Furthermore, since $\frac{\Delta v_g}{v_g} = \frac{R}{v_{ref}^2} P_{\text{loss}}$, then

$$\beta_1' = \beta_1 \left(1 + \frac{R}{v_{ref}^2} P_{\text{loss}}\right). \tag{13}$$

Consider an on resistance $r_{ds(on)}$ at the power switch S, a forward voltage drop V_{fw} at the diode d, and an equivalent series resistance (ESR) r_{L1} and r_{L2} at the inductor L_1 and L_2, respectively. Then, the average power loss under this condition is given by

$$\begin{aligned} P_{\text{loss}} &= \frac{v_g + v_{ref}}{v_g}\left(i_{L1}^* + i_{L2}^*\right)V_{fw} + \left(\frac{v_g + v_{ref}}{v_g}\right)^2 \left(i_{L1}^* + i_{L2}^*\right)^2 r_{ds(on)} \\ &\quad + \left(\frac{v_g + v_{ref}}{v_g}\right)^2 {i_{L1}^*}^2 r_{L1} + \left(\frac{v_g + v_{ref}}{v_g}\right)^2 {i_{L2}^*}^2 r_{L2} \\ &= \frac{v_g + v_{ref}}{v_g}\left(\frac{v_{ref}^2}{Rv_g} + \frac{v_{ref}}{R}\right)V_{fw} + \left(\frac{v_g + v_{ref}}{v_g}\right)^2 \left(\frac{v_{ref}^2}{Rv_g} + \frac{v_{ref}}{R}\right)^2 r_{ds(on)} \\ &\quad + \left(\frac{v_g + v_{ref}}{v_g}\right)^2 \left(\frac{v_{ref}^2}{Rv_g}\right)^2 r_{L1} + \left(\frac{v_g + v_{ref}}{v_g}\right)^2 \left(\frac{v_{ref}}{R}\right)^2 r_{L2} \\ &= \frac{v_{ref}\left(v_g + v_{ref}\right)^2}{Rv_g^2}\left(V_{fw} + \frac{v_{ref}}{Rv_g^2}\left(\left(v_g + v_{ref}\right)^2 r_{ds(on)} + v_g^2 r_{L2} + v_{ref}^2 r_{L1}\right)\right) \end{aligned}. \tag{14}$$

Consequently, substituting (14) into (13), therefore

$$\beta_1' = \beta_1 \left(1 + \frac{\left(v_g + v_{ref}\right)^2}{v_g^2 v_{ref}}\left(V_{fw} + \frac{v_{ref}}{Rv_g^2}\left(\left(v_g + v_{ref}\right)^2 r_{ds(on)} + v_g^2 r_{L2} + v_{ref}^2 r_{L1}\right)\right)\right). \tag{15}$$

Therefore, to adapt the *Switching Control Law 2* in practice and to overcome the issue of the steady-state output voltage error, β_1 needs to be replaced with β_1'. To evaluate the effectiveness of the proposed switching control law, a design example and the simulation results are presented in Section 4.

4. Design Example and Simulation Results

With the smartphone charging application in mind, we choose the converter parameters, as shown in Table 1. The typical rated voltage to charge a smartphone battery is 5 V, therefore it is the selected reference output voltage v_{ref} for the

converter. Meanwhile, 2 A is the typical rated current hence the load resistance R is set to 2.5 Ω. As for the non-ideal parameters $r_{ds(on)}$, r_{L1}, r_{L2}, and V_{fw}, they are realistically defined based on the datasheet in [30]-[32].

Table 1. DC-DC Zeta converter parameters.

Parameter	Value
v_g	18 V
$v_o\left(v_{ref}\right)$	5 V
R	2.5 Ω
L_1	100 μH
L_2	100 μH
C_1	100 μF
C_2	220 μF
f	100 kHz
$r_{ds(on)}$	0.16 Ω
r_{L1}	33 mΩ
r_{L2}	33 mΩ
V_{fw}	0.52 V

Table 2. Input voltage perturbation setup.

Input voltage v_g	Ave. input power P_g	Ave. input current I_g	Load resistance R
18 V	10 W	0.56 A	2.5 Ω
9 V	5 W	0.56 A	5 Ω
4.5 V	2.5 W	0.56 A	10 Ω

On the other hand, the input voltage v_g is assumed to be generated from photovoltaic (PV) panel with 10 W power rating. By looking at the 10 W PV datasheet [33], the typical voltage and current during maximum power generation are 18 V, and 0.56 A, respectively. Based on the characteristic of the PV [34], if less power is generated due to the low temperature and assumed that the irradiance remains constant at 1000 W/m^2, the current remains constant, but the voltage will be decreased. With this fact, we reflect the decrease of the input voltage v_g to the load resistance R with the assumption of zero power loss. For example, when input voltage v_g reduces to 9 V, since the average input current I_g is constant at 0.56 A, this gives an indication that the average input power P_g is 5 W ($P_g = I_g v_g$). Assuming all the input power P_g is transferred to the output/load, this is equivalent to the load resistance R of 5 Ω. For other examples, refer to **Table 2**.

To have a full on-line computation capability, in addition to the four state variables i_{L1}, i_{L2}, v_{C1}, and v_{C2}, two other variables are measured namely the input voltage v_g and the load current i_o, In practice, it is highly favorable to have less computation burden. As such, the parameters that are fixed are computed off-line

to reduce unnecessary on-line computation. Moreover, the floating number is avoided to achieve fast computation especially if one wants to implement hybrid control digitally. Considering the criteria, with (4), Table 1 and $R = v_{C2}/i_o$, the following expressions are gathered.

$$\alpha_1(x) = v_g(i_{L1} + i_{L2}) - i_o v_{C2} - \frac{5i_o}{v_{C2}}(v_{C1} - 2v_{C2} + v_g + 5), \tag{16}$$

$$\alpha_2(x) = -5(i_{L1} + i_{L2}) - i_o v_{C2} + \frac{5i_o}{v_{C2}}\left(2v_{C2} + \frac{5v_{C1}}{v_g}\right), \tag{17}$$

$$\begin{aligned}\beta_1' = {} & \frac{1}{4(v_g+5)}\left(25\left(\frac{i_o}{v_{C2}}\right)^2 + 2v_g^2\right) \\ & \times\left(1 + \frac{33(v_g+5)^2}{1000v_g^2}\left(3 + \frac{i_o}{v_{C2}v_g^2}\left(160(v_g+5)^2 + v_g^2 + 25\right)\right)\right),\end{aligned} \tag{18}$$

$$\beta_2 = \frac{5}{4v_g(v_g+5)}\left(25\left(\frac{i_o}{v_{C2}}\right)^2 + 2v_g^2\right). \tag{20}$$

Following *Switching Control Law* 2, the hybrid control algorithm for the stabilization of the DC-DC Zeta converter is executed as follows:

Hybrid Control Algorithm
Define initial conditions: $Set = 1$, $Reset = 0$, $S = 0$, $currentS = 0$.
a) Measure i_{L1}, i_{L2}, v_{C1}, v_{C2}, v_g and i_o.
b) Compute α_1, α_2, β_1' and β_2 in (16), (17), (18) and (19), respectively.
c) If $\alpha_1(x) < \beta_1'$, assign $Reset = 0$, else $Reset = 1$.
If $\alpha_2(x) < \beta_2$, assign $Set = 0$, else $Set = 1$.
If $Set = 1$ and $Reset = 0$, assign $S = 1$,
else if $Set = 0$ and $Reset = 1$, assign $S = 0$,
else assign $S = currentS$, $currentS = S$.
Repeat (a) to (c).

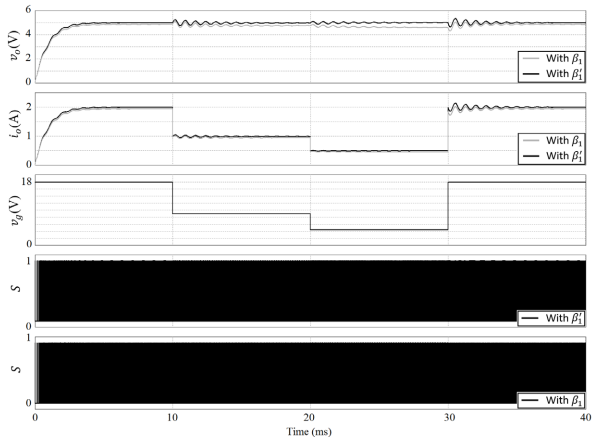

Figure 4. Simulation results under perturbations. Comparison of the responses from the hybrid control with the inclusion of β_1 or β_1'.

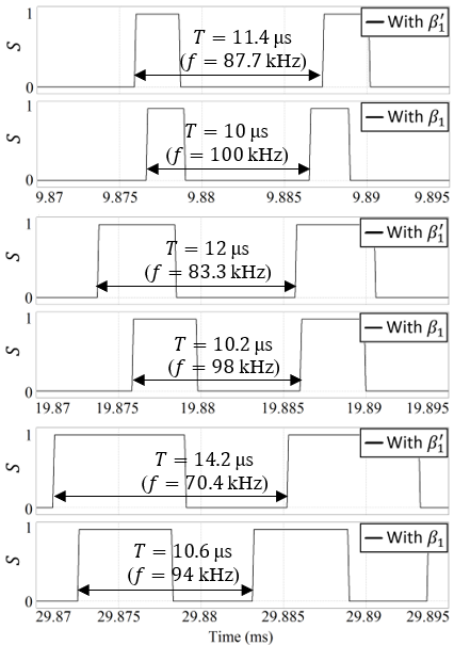

Figure 5. Close view (zoom in) of the steady-state switching signal at three-different time intervals.

Tested in PSIM®, the simulation results under the perturbations are shown in Figure 4. Initially, the input voltage is set to 18 V, and the corresponding load current is 2 A ($R = 2.5$ Ω). As can be observed, with the controller either utilizes β_1 or β_1', the output voltage settles at approximately 5 ms with no overshoot for both cases, with the different though is the former produces approximately −2.4% output voltage steady-state error ($v_o = 4.88$ V). At $t = 20$ ms, the input voltage abruptly drops to 9 V (−50%) which in turn reduces the output current to 1 A ($R = 5$ Ω). Although with the large input voltage perturbation, the effect in term of output voltage overshoot is quite minimal for both controllers (with β_1 or β_1') although some oscillations are found before they settle down at approximately t = 15 ms. However, the output voltage steady-state error increases to -4.6% ($v_o = 4.77$ V) for the controller with β_1. Moreover, at $t = 20$ ms, the input voltage drops further to 4.5 V and the output current becomes 0.5 A ($R = 10$ Ω). Interesting to note here is at this condition, the converter's operation changed from step-down (at $t = 0$ ms and $t = 10$ ms) to step-up thus highlight the usefulness of the Zeta topology which can handle two operation modes. The output voltage steady-state error (with β_1) is at its worst at −7.4% ($v_o = 4.63$ V) even though with less overshoot and oscillation as compared to previous case. On the contrary, in all the cases, the controller with β_1' provides a very good compensation in such that no output voltage steady-state error is observed.

So far, we have proved the effectiveness of the proposed hybrid control in regulating the output voltage even with the existence of large perturbation. Next, we want to confirm the correctness of the mathematical models in reducing the steady-state switching frequency. To begin with, let's have a look at the close view (zoom

in) of the switch S waveform in Figure 5. As seen in the figure, with the input power of 10 W, 5 W, and 2.5 W, the respected steady-state switching frequency for the controller with β_1 is 100 kHz, 98 kHz, and 94 kHz, whereas 87.7 kHz, 83.3 kHz, and 70.4 kHz, respectively, are recorded for the one with β_1'. As a reference, the pre-defined switching frequency is 100 kHz (refer to Table 1). Therefore, there are some discrepancies especially for the later controller. This is due to relatively lower efficiency at lower input power which in turn gives higher power loss thus from (13), this increases the magnitude of β_1'. Furthermore, since β_1' is inversely proportional to the switching frequency, lower switching frequency is expected. Nonetheless, the mathematical models guarantee the upper bound of the switching frequency thus preventing the arbitrary fast switching frequency from happening.

5. Conclusion

In this paper, we have presented output voltage stabilization with consideration of non-ideal DC-DC Zeta converter components. From the simulation results, it is shown that by taking into consideration the non-ideal properties of the Zeta converter in the switching control law formulation, the steady-state output voltage error is successfully eliminated. Furthermore, the upper bound of desired steady-state switching frequency is achieved. The above results make this research close to a practical environment. Nevertheless, the hardware experimental validation, as well as other input sources such as wind and thermal energy, will be investigated in future research.

Acknowledgements

The authors would like to thank Fakulti Teknologi dan Kejuruteraan Elektronik dan Komputer and Universiti Teknikal Malaysia Melaka for supporting this research.

Conflicts of Interest

The authors declare no conflicts of interest regarding the publication of this paper.

References

[1] Alvarez-Ramirez, J., Cervantes, I., Espinosa-Perez, G., Maya, P. and Morales, A. (2001) A Stable Design of PI Control for DC-DC Converters with an RHS Zero. *IEEE Transactions on Circuits and Systems I: Fundamental Theory and Applications*, **48**, 103-106. https://doi.org/10.1109/81.903192

[2] Vuthchhay, E. and Bunlaksananusorn, C. (2010) Modeling and Control of a Zeta Converter. *The* 2010 *International Power Electronics Conference*, Sapporo, 21-24 June 2010, 612-619. https://doi.org/10.1109/ipec.2010.5543332

[3] Chen, Z. (2012) PI and Sliding Mode Control of a Cuk Converter. *IEEE Transactions on Power Electronics*, **27**, 3695-3703. https://doi.org/10.1109/tpel.2012.2183891

[4] Garg, M.M., Hote, Y.V. and Pathak, M.K. (2015) PI Controller Design of a DC-DC Zeta Converter for Specific Phase Margin and Cross-Over Frequency. 2015 10*th*

Asian Control Conference (*ASCC*), Kota Kinabalu, 31 May-3 June 2015, 1-6. https://doi.org/10.1109/ascc.2015.7244716

[5] Nguyen, H., Maksimovic, D. and Zane, R. (2013) On/Off Control of a Modular DC-DC Converter Based on Active-Clamp LLC Modules. *IEEE Transactions on Power Electronics*, **30**, 3748-3760. https://doi.org/10.1109/compel.2013.6626413

[6] H. Sarkawi and Y. Ohta (2016) Optimal state-feedback and Proportional-Integral Controller Performance Comparison for Dc-dc Zeta Converter Operating in Continuous Conduction Mode. in Proc. SICE Annual Conf., 448-451.

[7] Sarkawi, H., Jali, M.H., Izzuddin, T.A. and Dahari, M. (2013) Dynamic Model of Zeta Converter with Full-State Feedback Controller Implementation. *International Journal of Research in Engineering and Technology*, **2**, 34-43. https://doi.org/10.15623/ijret.2013.0208005

[8] Olalla, C., Leyva, R., El Aroudi, A. and Queinnec, I. (2009) Robust LQR Control for PWM Converters: An LMI Approach. *IEEE Transactions on Industrial Electronics*, **56**, 2548-2558. https://doi.org/10.1109/tie.2009.2017556

[9] Olalla, C., Queinnec, I., Leyva, R. and El Aroudi, A. (2012) Optimal State-Feedback Control of Bilinear DC-DC Converters with Guaranteed Regions of Stability. *IEEE Transactions on Industrial Electronics*, **59**, 3868-3880. https://doi.org/10.1109/tie.2011.2162713

[10] Sarkawi, H. and Ohta, Y. (2017) Comparison of Conventional LQR and LMI based LQR Controller Performance on the DC-DC Zeta Converter with Parameters Uncertainty. *The 4th Multi-Symposium Control System*, Okayama, 6-9 March 2017, 642-647.

[11] Sarkawi, H. and Ohta, Y. (2018) Uncertain DC-DC Zeta Converter Control in Convex Polytope Model Based on LMI Approach. *International Journal of Power Electronics and Drive Systems*, **9**, 829-838. https://doi.org/10.11591/ijpeds.v9.i2.pp829-838

[12] Olalla, C., Leyva, R., Queinnec, I. and Maksimovic, D. (2012) Robust Gain-Scheduled Control of Switched-Mode DC-DC Converters. *IEEE Transactions on Power Electronics*, **27**, 3006-3019. https://doi.org/10.1109/tpel.2011.2178271

[13] Tan, S., Lai, Y.M., Tse, C.K., Martinez-Salamero, L. and Wu, C. (2007) A Fast-Response Sliding-Mode Controller for Boost-Type Converters with a Wide Range of Operating Conditions. *IEEE Transactions on Industrial Electronics*, **54**, 3276-3286. https://doi.org/10.1109/tie.2007.905969

[14] Guldemir, H. (2011) Study of Sliding Mode Control of DC-DC Buck Converter. *Energy and Power Engineering*, **3**, 401-406. https://doi.org/10.4236/epe.2011.34051

[15] Khasawneh, B., Sabra, M. and Zohdy, M.A. (2014) Paralleled DC-DC Power Converters Sliding Mode Control with Dual Stages Design. *Journal of Power and Energy Engineering*, **2**, 1-10. https://doi.org/10.4236/jpee.2014.22001

[16] Elkhateb, A., Rahim, N.A., Selvaraj, J. and Uddin, M.N. (2014) Fuzzy-Logic-Controller-Based SEPIC Converter for Maximum Power Point Tracking. *IEEE Transactions on Industry Applications*, **50**, 2349-2358. https://doi.org/10.1109/tia.2014.2298558

[17] Anand, R. and Mary, P.M. (2016) Improved Dynamic Response of DC to DC Converter Using Hybrid PSO Tuned Fuzzy Sliding Mode Controller. *Circuits and Systems*, **7**, 946-955. https://doi.org/10.4236/cs.2016.76080

[18] Cheng, Y., Du, H., Yang, C., Wang, Z., Wang, J. and He, Y. (2017) Fast Adaptive Finite-Time Voltage Regulation Control Algorithm for a Buck Converter System. *IEEE Transactions on Circuits and Systems II: Express Briefs*, **64**, 1082-1086.

https://doi.org/10.1109/tcsii.2016.2641924

[19] Alqudah, A., Malkawi, A. and Alwadie, A. (2014) Adaptive Control of DC-DC Converter Using Simulated Annealing Optimization Method. *Journal of Signal and Information Processing*, **5**, 198-207. https://doi.org/10.4236/jsip.2014.54021

[20] Cheng, K., Hsu, C., Lin, C., Lee, T. and Li, C. (2007) Fuzzy-Neural Sliding-Mode Control for DC-DC Converters Using Asymmetric Gaussian Membership Functions. *IEEE Transactions on Industrial Electronics*, **54**, 1528-1536. https://doi.org/10.1109/tie.2007.894717

[21] Wai, R. and Shih, L. (2012) Adaptive Fuzzy-Neural-Network Design for Voltage Tracking Control of a DC-DC Boost Converter. *IEEE Transactions on Power Electronics*, **27**, 2104-2115. https://doi.org/10.1109/tpel.2011.2169685

[22] Sreekumar, C. and Agarwal, V. (2007) Hybrid Control Approach for the Output Voltage Regulation in Buck Type DC-DC Converter. *IET Electric Power Applications*, **1**, 897-906. https://doi.org/10.1049/iet-epa:20070043

[23] Sreekumar, C. and Agarwal, V. (2008) A Hybrid Control Algorithm for Voltage Regulation in DC-DC Boost Converter. *IEEE Transactions on Industrial Electronics*, **55**, 2530-2538. https://doi.org/10.1109/tie.2008.918640

[24] Sreekumar, C. and Agarwal, V. (2006) Hybrid Control of a Boost Converter Operating in Discontinuous Current Mode. 2006 37*th IEEE Power Electronics Specialists Conference*, Jeju, 18-22 June 2006, 255-260. https://doi.org/10.1109/pesc.2006.1711772

[25] Ma, H.B. and Feng, Q.Y. (2009) Hybrid Modeling and Control for Buck-Boost Switching Converters. 2009 *International Conference on Communications, Circuits and Systems*, Milpitas, 23-25 July 2009, 678-682. https://doi.org/10.1109/icccas.2009.5250410

[26] Theunisse, T.A.F., Chai, J., Sanfelice, R.G. and Heemels, W.P.M.H. (2013) Hybrid Control of the Boost Converter: Robust Global Stabilization. 52*nd IEEE Conference on Decision and Control*, Firenze, 10-13 December 2013, 3635-3640. https://doi.org/10.1109/cdc.2013.6760442

[27] Theunisse, T.A.F., Chai, J., Sanfelice, R.G. and Heemels, W.P.M.H. (2015) Robust Global Stabilization of the DC-DC Boost Converter via Hybrid Control. *IEEE Transactions on Circuits and Systems I: Regular Papers*, **62**, 1052-1061. https://doi.org/10.1109/tcsi.2015.2413154

[28] Sarkawi, H. and Ohta, Y. (2019) The DC-DC Zeta Converter Hybrid Control Operating in Discontinuous Conduction Mode. 2019 *IEEE Conference on Control Technology and Applications* (*CCTA*), Hong Kong, 19-21 August 2019, 112-117. https://doi.org/10.1109/ccta.2019.8920515

[29] Sarkawi, H., Ohta, Y. and Rapisarda, P. (2021) On the Switching Control of the DC-DC Zeta Converter Operating in Continuous Conduction Mode. *IET Control Theory & Applications*, **15**, 1185-1198. https://doi.org/10.1049/cth2.12115

[30] https://www.vishay.com/docs/91019/irf530.pdf

[31] To Be Discontinued, Discontinued, Not Recommended and Obsolete. https://www.murata-ps.com/data/magnetics/kmp_1400.pdf

[32] Power Schottky Rectifier. https://www.st.com/resource/en/datasheet/stps10l60c.pdf

[33] https://www.parallax.com/sites/default/files/downloads/750-00032-18V-10W-Solar-Panel-Datasheet.pdf

[34] Souamy, R.M.D.L., Mimiesse, M.G., Yombi, B.L.N., Jiang, G., Hua, W., *et al.* (2024) Analysis of Maximum Powerpoint Tracking (MPPT) Adaptability in Inverters of the

Three-Phase Photovoltaic Systems Integrated into the Electrical Grid of Congo-Brazzaville. *Journal of Power and Energy Engineering*, **12**, 125-152.
https://doi.org/10.4236/jpee.2024.1211008